Keywords
Atmospheric Pressure Plasma (APP), Argon Plasma Jet, Boltzmann Plot, Stark Broadening, Spectroscopic Diagnostics, Biomedical Applications, Bacteria.

Authors
Ali Abdulhameed[1]
1Department of Physics, College of Education, University, Al-Qadisiyah, Iraq
Orcid: 0009-0007-9573-3889
E-mail: aliabd819@gmail.com

Ahmed H.Wanas[2]
2Department of Physics, College of Education, University, Al-Qadisiyah, Iraq
Orcid: 0000-0002-3011-0599
E-mail: ahmed.hmeed@qu.edu.iq

European Journal of Prosthodontics and Restorative Dentistry (2026) 34,7(s) 1198–1208

Optical Emission Spectroscopic Diagnostics and Physical Characterization of an Atmospheric-Pressure Argon Plasma Jet for Antibacterial Applications

Abstract
In this work a complete experimental study of properties of atmospheric pressure argon plasma jet is presented. The study is centered around performing an accurate spectroscopic diagnostics of the plasma for several operating conditions, especially consideration will be given to the effect of changing input power on the physical parameters of plasma.

Fundamental plasma parameters were calculated using Optical Emission Spectroscopy (OES). The plotting was plotted spectrally to quantize the argon atom lines of sight for Te. In addition, electron density ne was determined from analyzing the Stark broadening of the lines.

The results clearly indicated a direct relationship between higher input power and the temperature and number density of electrons. Furthermore, the efficacy of bio-plasma was evaluated based on selected bacterial microbiome. The findings showed that the produced plasma was more effective at killing bacteria, in that the rate of lethal action from increasing power and the ensuing rise in electron density correlating to a greater level of bacterial death.

The paper closes with a summary that power parameters are an important tool to control plasma properties for practical applications and sources, especially in the fields of sterilization and disinfection.

Received:05-06-2026
Revised:17-07-2026
Accepted:03-08-2026
Doi:10.1922/ejprd.v34i7s.1770

INTRODUCTION

Juvenile idiopathic arthritis remains the most prevalent chronic rheumatic disease of childhood and is an essentially

The field of non-thermal plasma applications has rapidly expanded over the last few years to include biomedical devices, biological materials, and material technology [1]. Atmospheric Pressure Plasma Jet is a non-thermal plasma type characterized by high-electron temperature and low gas temperature. Utilizing the gas flow generates a plasma plume with reactive species away from the electrodes [2]. Therefore, Atmospheric Pressure Plasma Jet (APPJ) gained significant advantages for its favorable properties in industrial applications such as materials, electronics, and polymer processing potential. APPJs may also be used in biomedical applications, including modern pharmaceutical therapies, injury healing and sterilization, and manufacturing applications such as etchings and living tissue treatment. By changing the (APPJ) configuration, the applied voltage and working gas, the plasma plume propensities blown outside the discharge tube and into the surrounding air can easily be controlled [3-4]. APPJs usually treat only a small area at a time (in order of mm2) in comparison with DBDs, which can treat several (or greater) cm2 surfaces [5]. The majority of plasma jets work in noble gasses like He and Ar, often with small molecular gas addition such as air, O2, and H2O to enhance the yield of reactive species. A plasma jet requires to operate in an air atmosphere for many applications, contributing to air diffusion in the jet effluent. As the plasma is known to affect the gas flow, uncontrolled air diffusion and entrainment in the plasma jet may result [6]. Optical emission spectroscopy (OES) is generally used for plasma diagnostics with low temperatures. This approach is relatively inexpensive, flexible, and intrusive. It enables the determination with the so-called Boltzmann plot technique of plasma parameters such as electron temperature and density. Spectral lines correspond to optical transitions between two atom/molecule quantum levels, and the spectral line intensity is determined by many gas species in the upper state. The density of numbers, in turn, depends on the temperature and density of the electron [7]. Many plasma jet devices producing a non-thermal atmospheric pressure plasma plume were studied in recent years. The interest of this subject is determined by the potential medical and economic advantage of many non-thermal plasma technologies. Thus, this study focuses on the characterization of cold atmospheric plasma (CAP) generated by a DC discharge in argon gas. The primary objective is to determine the physical parameters of the plasma such as electron temperature and density using optical diagnostic techniques. Furthermore, this data is utilized to evaluate the efficacy of the plasma as a biocidal agent against bacteria and biofilms on surfaces, with an emphasis on investigating the synergistic effects associated with variations in the applied electrical power.

2. METHODOLOGY

The electrons temperature (Te) is the most significant factor in describing the plasma state. Te can be calculated using the Boltzmann plot method as follows [8-9]:

$$Ln\left(\frac{I_{ji}\lambda_{ji}}{g_j A_{ji}}\right) = \left(-\frac{E_{k,z}}{K_B T_e}\right) + Ln\left(\frac{hcL_{nz}}{4\pi p_z}\right) \ldots\ldots\ldots\ldots\ldots\ldots\ldots. (1)$$

Where: Z represent the ionization state, h is Planck's constant, c is speed of light, KB is Boltzmann constant, j is the highest energy level, i is the lower energy level, λji is the wavelength corresponding to the transition between level j and level i for the same ionization degree, Aji the transition probability corresponds to transition from j to i, Iji is the intensity of transition from j to i, PZ is the species partition function in ionization stage Z, and gj is a statistical weight. The electron temperature was calculated by plotting the left-hand side of Equation (1) in comparison to the species' higher-level energy during the Z ionization phase, expressed in units of eV [10-11]. The electron temperature is determined from the slope (= -1/KBTe).

There are many methods adjusted to calculated the electron number density, the Stark broadening method is used in this work. The electron number density was determined using the Stark broadening method [12]:

$$n_e(cm^{-3}) = \left[\frac{\Delta\lambda_{stark}}{2\omega_s}\right] N_r \qquad (2)$$

where ωs is the electron impact, Δλ denotes the full width at half maximum of the line, Nr is the reference electron number density, that equal of 1016 cm-3 for neutral atoms and 1017 cm-3 for singly charged ions.

3. MATERIALS AND METHODS

3.1 Design of (APPJs) system

Fig. 1. illustrates the experimental design of an atmospheric pressure plasma jet (APPJs). The atmospheric pressure plasma jet consists of two electrodes. One electrode is a 15 cm long, 1 mm diameter stainless steel needle passing through a Teflon insulator and a 10 cm long, 8 mm diameter heat-resistant glass tube connected to the insulator so that the needle reaches the middle of the glass tube. The other electrode is a copper ring electrode, electrically connected with positive polarity, and positioned around the outside of the glass tube near its end. The two electrodes are electrically connected to a DC power supply with a maximum voltage of 23 KV and current 35 mA. Argon gas with 99% purity flows through a cavity within the insulator, through the glass tube, reaching outside of it, Electrical power was applied ranging between 200 to 300 Watt. The high-voltage input is connected to the steel needle electrode and the ring electrode to produce the atmospheric pressure plasma jet of argon. The gas emitted from the argon cylinder was read by a suitable flow velocity meter. An argon discharge was generated between the electrodes when a DC voltage was applied and the argon flow rate was set to a specific value. The argon discharge between the electrodes occurred at atmospheric pressure. The

emission spectrum of the discharge was focused onto a probe aperture connected to the spectrometer via an optical fiber. The spectrometer was then connected to a computer via a cable to measure the emission lines of the argon spectrum. The NIST database software was used to estimate the characteristics of the argon plasma jet [13] shows in table (1).

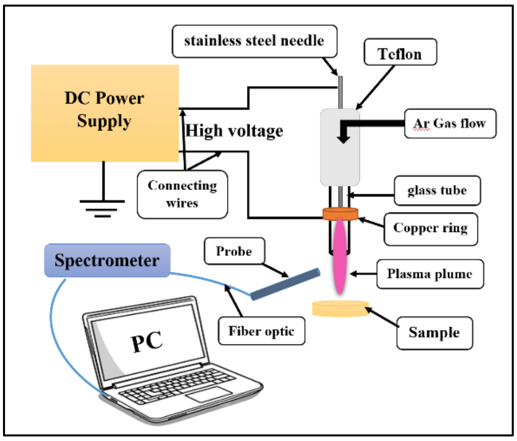

Fig. 1. Schematic setup of the Atmospheric pressure plasma jets (APPJs)

TABLE 1. Spectroscopy of the parameters of the measured spectral lines emitted from Ar plasma jet corresponding to the NIST database [13].

Emmision Lines	λ (nm)	GkAik (s-1)	Ek (eV)
Ar I	751.4	4 × 107	13.27
	763.5	1.22 × 108	13.17
	826.4	4.59 × 107	13.32
	842.4	4.17 × 107	13.28

The emissions of the plasma plume were analyzed using a wide-range spectrometer (S3000-UV-NIR) with a spectral resolution of 0.1 nm and a wavelength range of (161.95-1081.18) nm. Fig. 2. show an optical spectrum analyzer equipment used in the work.

Fig 2. show the optical emission spectrophotometer used in the work

3.2 Sample preparation and handling
3.2.1 Bacterial Preparation
Three clinical bacterial isolates were selected for this study: Escherichia coli (E. coli) and Enterobacter cloacae (E. cloacae) as Gram-negative bacteria, and Staphylococcus aureus (S. aureus) as a Gram-positive bacterium. The strains were initially activated by culturing in a nutrient broth for 24 hours at 37°C in an incubator Fig.3. Subsequently, the isolates were inoculated onto nutrient agar plates and incubated for 24 hours at 37°C to obtain pure colonies.
3.2.2 Plasma Treatment Protocol
The bacterial colonies were exposed to argon plasma jets at varying input power levels. To ensure experimental reproducibility and consistency, other operational parameters were kept constant as follows:

- Gas flow rate: 5 L/min
- Exposure time: 2 minutes

- Treatment distance (nozzle-to-sample): 10 mm

Fig. 4. shows an operational image of one of the samples during direct exposure of the bacteria samples to plasma jet. Gas control group was set up to verify the experimental result and obtain the plasma effect separately. In this group, the bacterial samples were subjected to an identical argon gas flow rate (5 L/min) over an equal duration without inducing the plasma discharge. This avoid the gas flow contribution to any inactivation observed biological.

Fig. 3. shows the incubator used in operation.

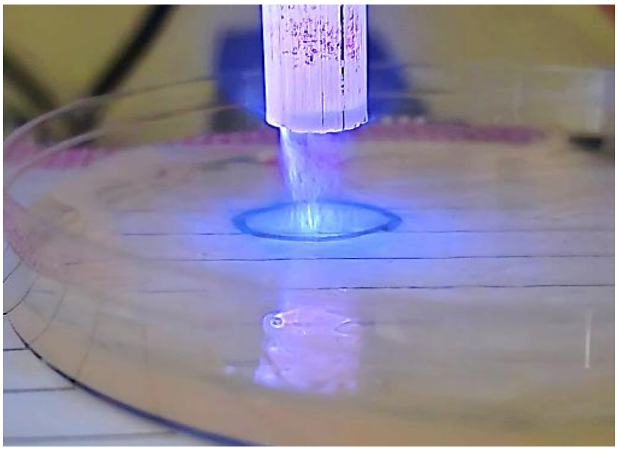

Fig. 4. is an image of one of the samples during direct plasma exposure.

3.3 Measurements

3.3.1 Bacterial adhesion

The ability for bacterium to adhere was assayed via detachment assay. In short, you were incubated the bacterial suspensions with inert polymer granules for specific periods of time to allow adhesion. The granules were then transferred to saline-containing tubes and treated by sonication Fig. 5. Minutes to allow the bacteria that have adhered to detach. The optical density (OD) of the suspended bacteria in the saline solution was subsequently determined by passing through a UV-V is spectrophotometer Fig. 6. This measurement permitted comparison on the human scale of the adhesion levels between plasma-treated samples with that of control.

Fig. 5. Ultrasonic bath employed for the detachment of adhered bacteria from the surface of inert polymer granules

Fig. 6. UV-Vis spectrophotometer used to read the OD of suspensions in order to assess the degree of adhesion (OD).

Colony counting method was used to evaluate the bacterial adhesion. Following plasma treatment, the bacteria were rinsed off from the surface and twofold serially diluted and plated onto agar medium. The results was expressed as Colony Forming Units per milliliter (CFU/mL) and denotes the number of live cells that can reproduce.

3.3.2Biofilm formation examination

The biofilm formation was evaluated by the crystal violet staining assay method. Both control and plasma-treated bacterial suspensions were added to 96-well microtiter plates and incubated for 24h at 37◦C. Removes the culture medium, followed by washing with phosphate-buffered saline (PBS) to remove non-adherent planktonic cells after incubation. Then, the biofilm left was fixed and stained with a crystal violet solution. After washing off the excess stain, solubilization of bound crystal violet dye was performed with 95% ethanol. The absorbance of solubilized dye was determined by a microplate reader at 600 nm wavelength Fig. 7. This methodology gave a common quantification parameter to compare biofilm density in various plasma treatments and the control.

Fig. 7. Thermo Scientific Multiskan FC microplate reader used for the quantitative assessment of biofilm density via optical density (OD) measurement of crystal violet-stained samples.

Biofilm biomass was measured as the OD at 600 nm using the crystal violet assay.

4. RESULTS AND DISCUSSION

4.1 Plasma Jet Properties

4.1.1 Morphological and Physical Parameters

4.1.1.1 Plasma Jet Temperature (Gas Temperature)

Thermal characterization of plasma jet was achieved utilizing a high-resolution thermocouple sensor (accuracy ± 0.1oC) placed at the nozzle exit. Here, we found a gas temperature in the vicinity of room temperature that fits perfectly with known criteria for safe plasma-tissue interaction. Moreover, a thermal safety confirmation was for obvious design on human skin, which demonstrated no thermal injury occurred maintaining the jet suitable for biomedical application Fig. 8.

Visual inspection of the plasma jet shows that the discharge propagates not as a continuous, homogeneous column but as a filamentary structure made of discrete electron current channels. This filamentary nature comes from the intrinsic instabilities of the discharge path in this Direct Current (DC) atmospheric pressure discharge regime. Current does not evenly distribute over the nozzle cross-section, instead squeezing into local conductive micro-channels. The formation of these distinct filamented electron currents rather than a continuous plasma column is produced from the flow gas interacting with an electric field, which causes local pathways of resistance to be low, i.e. ionization occurs in localized regions that have less hindrance to the flow of electrons.

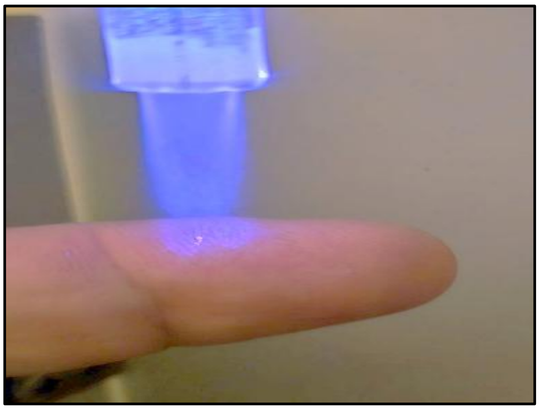

Fig. 8. A photo showing cold atmospheric plasma jet impacting onto cutaneous human layer, indicating the non-thermal identity of plasma discharge.

4.1.1.2 Jet Length

Figure 8 shows the relationship between input power and plasma jet length, where the gas flowing rate was fixed at 2 L/min experimental results exhibit a consistent positive correlation. The obtained jet length increased significantly from 27 to 29 mm Fig. 9. The stretch is mainly due to the increased ionization rates and electron density caused by the higher input energy. This in turn expedites the generation and propagation of reactive species leading to a longer plasma column. The advantage of this expansion is notable in a therapeutic light, as it leads to an enlarged effective area to treat and an increased flux of active species delivery to the bacterial target.

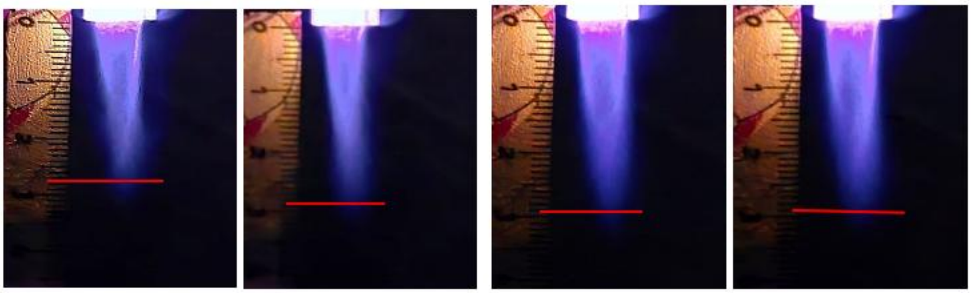

Fig. 9. Experimental images demonstrating the variation of plasma jet length at different input power levels (200– 300) Watt, with a constant gas flow rate of 2 L/min.

4.1.2 Optical Emission Spectroscopy (OES)

Plasma spectroscopy focusing on low-temperature plasma atomic and molecular emission spectroscopy is a powerful diagnostic tool for Ar plasma parameter determination. This technique's main premise is that the intensity of light emitted from an excited state at specific wavelengths is proportion to the species' density. The light intensity measurement gives a qualitative indication of the concentration to the species involved in optical emissions. Plasma species collide with electrons and other plasma species in the atmospheric plasma jets. Collisions of excitation and decay in radiative species emit plasma species characteristics that can detected and analyzed as optical emission spectroscopy (OES) [14]. These plasma emission intensities provide information about the plasma species concentration. The data provided in Table 1 have been used in this study and discussion of spectral lines emitted atoms. Depending on optical emission spectra (OES) of the Ar plasmas jet. The behavior of an argon plasma jet at atmospheric pressure was studied at different powers.

Fig. 10. illustrates the optical emission spectrum of the 300 W plasma discharge. The spectrum is dominated by high-intensity argon (Ar I) atomic emission lines within the 696–850 nm range, confirming the role of argon as the primary carrier gas. Additionally, molecular nitrogen (N2) bands are widely visible in the 337-435 nm range explaining a lot of the molecular activity. On the other hand, those reactive radical species such as hydroxyl radical (OH) at 308.9 nm, nitric oxide (NO) (200-300) nm and atomic oxygen O I at (777.54 nm) [15]. also emerge but more or less weak emissions than argon and nitrogen lines. The low-intensity detection can be explained by their short lifetime and typically lower concentrations than the main species. Even if they are of lower intensity, the detection of these radicals is important because they are the basic active agents involved in the oxidative reaction with and destruction of the structure of a biofilm.

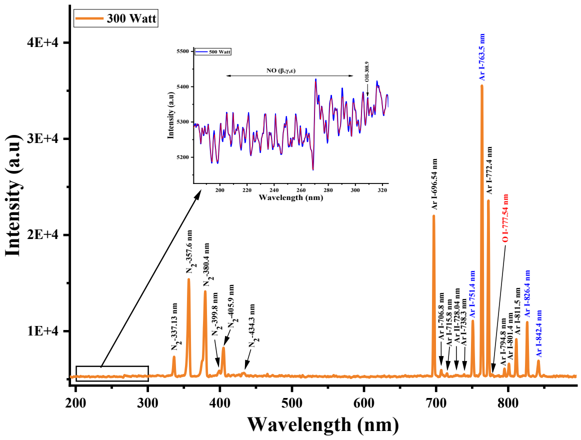

Fig. 10. shows the optical emission spectrum of the 300 Watt plasma discharge.

From the spectroscopic analysis, we observed that there is a strong positive linear correlation between input electrical power and the intensity of the emitted spectral lines Fig. 11. This increase in intensity of the spectral peaks is largely due to the influence of power levels on both electron density and electron temperature (Te) which alters considerably the population distribution of the corresponding excited energy states. Higher energy input causes a larger rate of inelastic scattering between electrons and argon atoms, which allows more excitation and de-excitation. As a result, the concentration of atoms in excited states is increased, resulting emission photons at higher intensities and larger spectral peaks as previously shown by source [16]

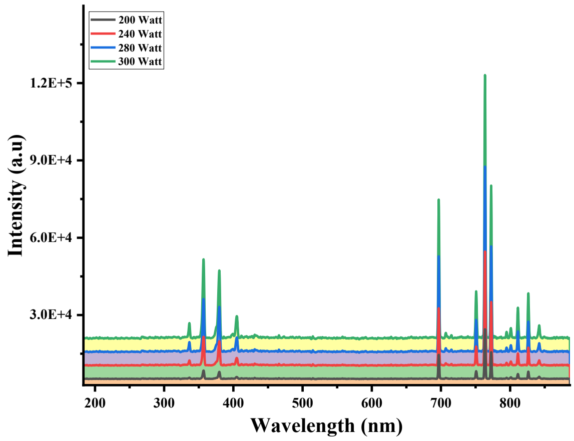

Fig. 11. Wavelength vs Intensity of spectral line at different input powers

4.1.3 Calculation of Plasma parameters (Te - ne)

A group of neutral argon (Ar I) spectral lines with wavelengths 751.4, 763.5, 826.4 and 842.4 nm were chosen for the precise determination of the electron temperature (Te). These lines were specifically selected based on their spectral intensity, signal-to-noise ratio (SNR), and the existence of an accurate atomic constants [transition probabilities Aki, statistical weights gk] in NIST ensured that data with potential computational error was minimized. Fig. 12. shows Boltzmann plots at various power levels, indicating the linear distribution of data points proves the applicability of the Boltzmann model in these experimental conditions. Electron temperature was then calculated from the slope of these linear fits.

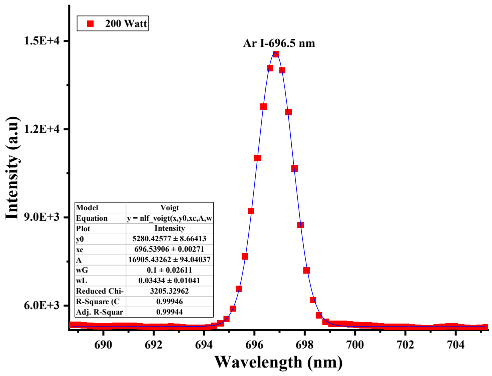

Fig. 12. Boltzmann plot different input powers.

To accurately determine the electron density (ne) in the argon plasma, the Ar I spectral line at 696.5 nm was selected due to its high sensitivity to the Stark broadening effect. Under operating conditions where the electron temperature is approximately 5000 K, an electron impact parameter of 0.00409 was adopted [17]. The spectral line was analyzed, and the Full Width at Half Maximum (FWHM) was extracted using OriginLab software via curve fitting analysis, where the Lorentzian component obtained from the fitting process was considered the actual Stark broadening value. Other minor broadening contributions (e.g., natural and Doppler broadening) were deemed negligible, given their small values ranging from 0.04 to 0.07 nm compared to the Stark broadening under the current operating conditions [18]. Fig. 13. illustrates a representative example of the fitting process used to extract the FWHM.

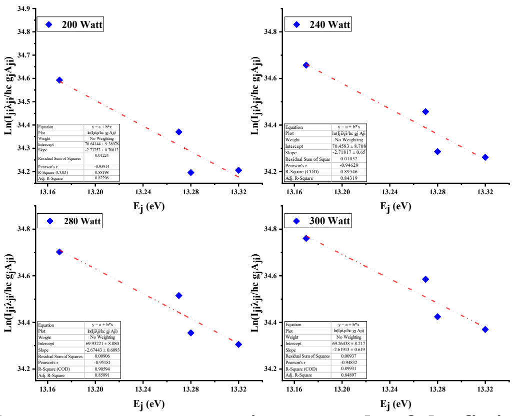

Fig. 13. illustrates a representative example of the fitting process used to extract the FWHM.

Fig. 14. shows that the increased input power leads to an increase in Stark line width, which is in accordance with the same trend of electron density. The increase of the Full Width at Half Maximum (FWHM) of the spectral line with increasing electrical power is explained mainly by an increase in electron density (ne) explainably in argon plasma discharge. The more input power we have, the more ionization will be in large numbers of electrons present. As Stark broadening which is the principal mechanism under presently used conditions varies linearly with electron density, a rise in collisions events between electrons and the radiating atoms lead to widen of spectral lines again, this phenomenon will be reflected as an increasing of (FWHM) [19].

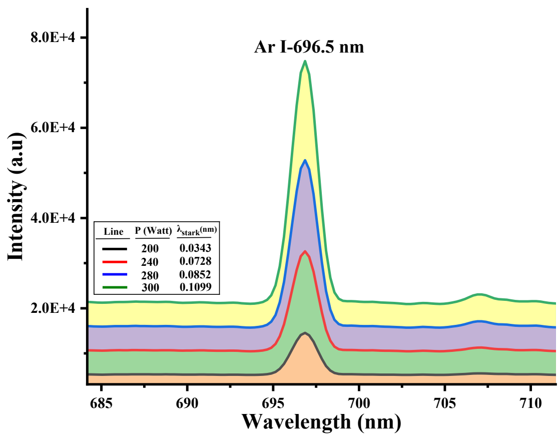

Fig. 14. The Stark beam expands as the power is swept up.

ejprd.org - Published by Riset Publishing Services LLC

Fig. 15. shows the variation of the fundamental plasma parameters electron temperature (Te) and electron density (ne) with respect to input electrical power. Results strongly show that the electrical power influences both physical parameters in a linear way: increasing this power yields to a significant increase of both electron temperature and electron density.
This phenomenon can be physically explained with:
First: The sublocal electron temperature (Te) increase
This increase in Te results from a higher E field applied to the plasma thereby transferring more energy into electrons. When we increase the power, therefore, the electric field contributes to accelerating electrons and giving them additional kinetic energy prior to their collisions with neutral gas atoms. Naturally, this results in a higher value of the mean electron temperature [16,20].
Second: Increase by electrons density (ne):
The increase in ne is due to the increased efficiency of participant ionization processes. As the electron temperature and kinetic energy increase, elastic collisions of electrons with neutral argon atoms become more frequent and energetic, producing elastic collisions that lead to ionization of even more argon atoms. This process creates additional electron-ion pairs and thus increases the total density of free electrons in the discharge volume [20,21].

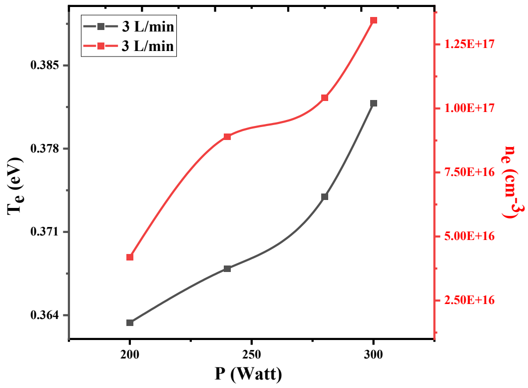

Fig. 15. Variation of variables electron temperature (Te), electron density (ne) with respect to input power(P) at constant fixed gas flow rate 3 L/min.

4.2 Bio-application Plasma Jet

The experiments were carried out in preparation, to see the impact of argon gas flow on the bacterial samples. There was no effect on bacterial viability (compared to untreated control), indicating that the argon gas flow itself does not have a direct involvement in the process of bacterial inactivation. Thus, all biological effects seen through the following experiments are those caused by the plasma discharge itself.
All (S. aureus, E. cloacae, and E. coli) tested biofilm strains exhibited a clear inverse relationship between the applied plasma input power and the residual biofilm biomass as established through our experimental results Fig Inhibition rates by type are shown in Figure 16. This is inherently related to plasma parameters selected in diagnostics.
Spectroscopic analysis confirmed that increasing the input electrical power resulted in significant increases in both electron density (ne) and electron temperature (Te). Consequently, this physical improvement contributes the inelastic collision rate and produce an enhanced flux of reactive oxygen and nitrogen species (RONS) such as hydroxyl radical (OH), nitric oxide (NO) and atomic oxygen detected in OES spectra. This finding confirms that the increased levels of RONS produced will be correlated with the higher power levels and this is the main mechanism of action contributing to biofilm eradication performance [22].
Biofilm destruction suffered from a synergistic mechanism of chemical etching and oxidative stress [23]:
EPS Matrix Degradation: The generated RONS act by decomposing the extracellular polymeric substances (EPS) matrix—the protective biological barrier of the biofilm—through direct chemical oxidation.
Cellular Damage: These reactive agents penetrate the bacterial cell wall, inducing severe oxidative stress, lipid peroxidation, and DNA damage, which compromise cell membrane integrity and lead to cell lysis.
In addition, the difference in decay rates among strains is also striking. The Gram-negative strains (E. coli and E. cloacae) are more sensitive to plasma treatment than the Gram-positive S. aureus. Dissimilar responses from Gram-positive and -negative strains are primarily attributed to differences in cell wall structure, specifically the higher density of peptidoglycan found in S. aureus confers greater structural rigidity against plasma-mediated oxidative stress unlike the more porous cell walls of other Gram-negative species that provide vulnerabilities for faster penetration and destruction by permeabilizing reactive species [24].

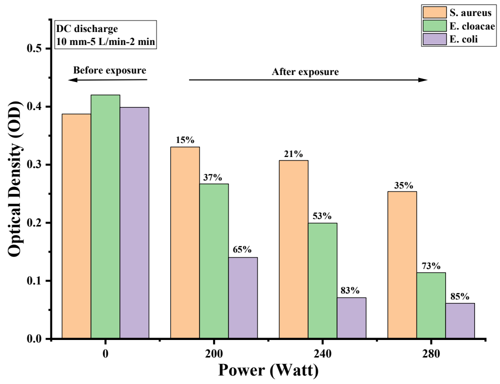

Fig. 16. Optical Density (OD) of S. aureus, E. cloacae and E. coli biofilms were based on different plasma input power with respect to inhibition rates for each one type respectively.

Fig. 17. shows the data of bacterial adhesion as a function to increasing input power (Anti-adhesion efficiency ratios) for control and plasma treated group and interestingly we can see different three strains responses. As evident from the control (0 W) group, the Gram-positive strain (S. aureus) gave less adhesion at baseline levels compared with the two Gram-negative strains, E. coli and E. cloacae in this work. The initial trend was reversed for Gram-negative bacteria compared to the Gram-positive strain after exposure of plasma at increased power; and they were much less adhesive than Gram-positive colonies at higher powers.

This indicates that although the Gram-negative strains have higher inherent adhesion characteristics, they are more vulnerable to subsurface damaging action of plasma-induced reactive species (RONS). This differential response is explained based on unique cell wall architectures with the outer membrane of Gram-negative bacteria lacking the physical barrier mechanism provided by the thick peptiodglycan layer of S. aureus, rendering them more susceptible to oxidative stress and bacterial membrane disruption [25].

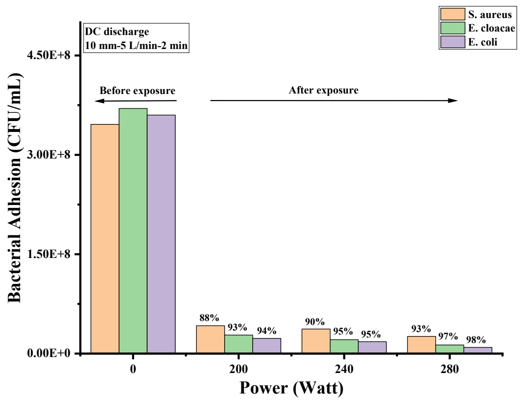

Fig. 17. Plasma power effects on the bacterial adhesion (CFU/mL) vs. S. aureus, E. cloacae and E. coli strains (Anti-adhesion efficiency ratios).

5. CONCLUSIONS

A cold atmospheric pressure plasma (APP) jet was developed and characterized as a potential biomedical device for clinical applications. From the experimental results, we can conclude that:

1.Thermal Safety and Non-Thermal Nature: The macroscopic thermal diagnostics consisting of all the probe measurements as well as manual tactile evaluation confirmed that the plasma jet operates in a near room temperature region. This so-called 'cold' character determines the plasma as being a very useful instrument for direct treatments of biological tissues without any thermal damage.

2.Tunable Plasma Parameters: A measurable relationship was observed between the power to plasma and its discharge characteristics. At higher input power, it is the length of plasma plume that increases and also a sharp rise in electron temperature (Te) and then in electron density (ne). This shows the plasma discharge can be well modulated to the point of generating reactive species at the desired intensity.

3.Extremely Efficient Biofilm Eradication and Adhesion Inhibition: the biological experimental application indicated that the plasma jet working as an extreme effective weapon against Gram-positive and -negative bacteria. Our results showed that a decreasing relationship between plasma input power and biofilm thickness or bacterial adhesion capacity was observed. In particular, higher power levels (higher concentrations of reactive species) both significantly decreased biofilm structural integrity and inhibited adherence.

4.The results indicate that the mechanism of action is mainly due to synergy between reactive oxygen and nitrogen species (RONS). This plasma-induced oxidative stress sufficiently disrupts the bacterial cell wall and EPS (extracellular polymeric substances) matrix, forming a promising multi-germ spectrum sterilization and anti-biofilm system.

ACKNOWLEDGEMENTS

The study was funded by the Department of Plasma Physics, College of Education, Al-Qadisiyah University in cooperation with the Department of Medical Biotechnology, College of Biotechnology.

REFERENCES

1. H.B. Baniya, R. Shrestha, R.P. Guragain, M.B. Kshetri, B.P. Pandey, D.P. Subedi, Int. J. Polym. Sci., 2020 (2020) 1-7.
2. A. Segat, N.N. Misra, P.J. Cullen, N. Innocente, Food and Bioprod. Process., 98 (2016) 181-188.
3. F. Liu, B. Zhang, Z. Fang, M. Wan, H. Wan, K.K. Ostrikov, Plasma Process. Polym., 15(1) (2018) 1-11.
4. X. Li, C. Di, P. Jia, W. Bao, Plasma Sources Scie. Technol, 22(4) (2013) 093516.
5. A.M. Lietz, X. Damany, E. Robert, J.-M. Pouvesle, M.J. Kushner, Plasma Sources Scie. Technol., 28(12) (2019) 1-57.
6. S. Yatom, Y. Luo, Q. Xiong, P.J. Bruggeman, Appl. Physi., 50(41) (2017) 415204.
7. K.E. Evdokimov, M.E. Konischev, V.F. Pichugin, Z. Sun, Resource-Efficient Technologies, 3(2) (2017) 187-193.
8. A. K. Bard and Q. A. Abbas, Optik 272, 170346 (2023).
9. Sami, W. A., Khadayier, A. A., & Shaheed, M. A. (2026). Synthesis and PVP Coating Effects on Cadmium Ferrites for Antibacterial Applications. Iraqi Journal of Science, 1580-1587.
10. U. S. Inan and M. Gołkowski, Principles of Plasma Physics for Engineers and Scientists (Cambridge, UK, Cambridge University Press, 2010).
11. S. Waheed, S. Bashir, A. Dawood, S. Anjum, M. Akram, A. Hayat, S. Amin, and A. Zaheer, Optik 140, 536 (2017).
12. A.M. El Sherbini et al., “Measurements of plasma electron temperature utilizing magnesium lines appeared in laser produced aluminum plasma in air”, Opt. Photon. J., 2(04) (2012) 278.
13. NIST Atomic Spectra Database, http://www.nist.gov/pml/data/asd.cfm, (21.12.2016).
14. Mohammed, Raghad S., Kadhim A. Aadim, and Khalid A. Ahmed. "Estimation of plasma parameters in a DC atmospheric pressure Argon plasma jet." AIP Conference Proceedings. Vol. 2386. No. 1. AIP Publishing LLC, 2022.
15. Barkhordari, Ali, et al. "Influence of the argon admixture on the reactive oxide species formation inside an atmospheric pressure oxygen plasma jet." Scientific Reports 14.1 (2024): 3425.
16. Giannakaris, Nikolaos, et al. "Optical emission spectroscopy of an industrial thermal atmospheric pressure plasma jet: Parametric study of electron temperature." Spectrochimica Acta Part B: Atomic Spectroscopy 207 (2023): 106736.
17. Dong, Lifang, Junxia Ran, and Zhiguo Mao. "Direct measurement of electron density in microdischarge at atmospheric pressure by Stark broadening." Applied Physics Letters 86.16 (2005).
18. Aadim, Kadhim A., et al. "Influence of gas flow rate on plasma parameters produced by a plasma jet and its spectroscopic diagnosis using the OES technique." IOP Conference Series: Materials Science and Engineering. Vol. 987. No. 1. IOP Publishing, 2020.
19. Al-Helaly, M. T., Hussain, S. A., & Shaheed, M. A. (2025). Investigation of Structural and Optical Properties of Palladium–Copper Nanoparticles Synthesized by Pulsed Laser Ablation Method for Biomedical Applications. J. Appl. Bioanal, 11, 521-531.
20. Barkhordari, A., et al. "Study of the physical discharge properties of a Ar/O2 DC plasma jet." Indian Journal of Physics 92.9 (2018): 1177-1186.
21. Yugeswaran, Selvarajan, and V. Selvarajan. "Electron number density measurement on a DC argon plasma jet by stark broadening of Ar I spectral line." Vacuum 81.3 (2006): 347-352.
22. Rao, Yifan, et al. "Fighting mixed-species microbial biofilms with cold atmospheric plasma." Frontiers in microbiology 11 (2020): 1000.
23. Fallon, Muireann, et al. "The effect of cold plasma operating parameters on the production of reactive oxygen and nitrogen species and the resulting antibacterial and antibiofilm efficiency." Plasma Medicine 12.1 (2022).
24. Mai-Prochnow, Anne, et al. "Gram positive and Gram negative bacteria differ in their sensitivity to cold plasma." Scientific reports 6.1 (2016): 38610.
25. Lee, Myung-Jin, et al. "The antibacterial effect of non-thermal atmospheric pressure plasma treatment of titanium surfaces according to the bacterial wall structure." Scientific reports 9.1 (2019): 1938.